

Relative Jump Distance: a diagnostic for Nested Sampling

Johannes Buchner^{1*}

Max Planck Institute for Extraterrestrial Physics, Giessenbachstrasse, 85748 Garching, Germany

Received xx, Accepted xx

ABSTRACT

Nested sampling is widely used in astrophysics to reliably infer model parameters and compare models within a Bayesian framework. To address models with many parameters, Markov Chain Monte Carlo (MCMC) random walks are used within nested sampling to advance a live point population. Diagnostics for nested sampling inference are essential to verify that trustworthy astrophysical conclusions can be drawn. We develop a diagnostic to identify problematic random walks that do not meet the requirements of nested sampling. The distance from the start to the end of the random walk, the jump distance, is compared to the typical neighbour distance between live points, to obtain a relative jump distance (RJD). A robust estimate of a typical neighbour Mahalanobis distance is obtained with the MLFriends algorithm. In mock and real-world inference applications such as inferring the distance to GW170817, we observe the relative jump distance. We propose the geometric mean RJD and fraction of RJD>1 as new summary diagnostics. Problematic nested sampling runs are identified as those that differ significantly from reruns with much longer MCMC chains, and used to test the sensitivity of these summary diagnostics. Problematic inference runs are consistently associated with low average RJDs and $f(\text{RJD}>1)$ below 50 per cent. The RJD is more sensitive than previous tests based on the live point insertion order. The RJD diagnostic is proposed as a widely applicable diagnostic to verify inference with nested sampling. It is implemented in the UltraNest package in version 4.1.

Key words. Nested Sampling; Markov Chain Monte Carlo

1. Introduction

Nested sampling (Skilling 2004; Ashton et al. 2022) is a widely used algorithm in astrophysics to infer model parameters and compare models within a Bayesian framework. To illustrate, the popular packages (Feroz et al. 2009; Handley et al. 2015; Speagle 2020; Buchner 2020) have over 3500 citations to date, supporting a wide range of scientific endeavours. One appeal of nested sampling is its robustness to complex parameter degeneracies, frequently encountered in limited astronomical data.

Nested sampling achieves this by sampling a population of K live points from the prior probability distribution. Then, at each iteration, a live point is discarded and replaced with a new prior-sample, under the constraint that its likelihood must exceed the likelihood of the recently discarded point. This induces the behaviour of the live point population being distributed throughout the parameter space, but progressing towards the best fit. The key insight of Skilling (2004) is that each iteration of nested sampling discards a constant fraction of the prior probability mass at each iteration, $\delta \approx 1/K$. The posterior distribution can be approximated by the discarded points, weighed by $w_i = L_i \times V_i$, where $V_i = \delta \times (1 - \delta)^i$ is the approximated prior probability discarded at iteration i , and L_i is the likelihood of the discarded point. Then, the marginal likelihood is $Z \approx \sum w_i$. For a more detailed introduction to nested sampling, see Ashton et al. (2022).

Several approaches have been proposed for prior-sampling under the likelihood constraint. The original proposal by Skilling (2004) is to start a random walk from a live point for a number of steps M , and adopt the final point as a new live point. Points are accepted if they exceed the current likelihood threshold. Such step sampling nested sampling is the most efficient approach for

models with many parameters (say, 20 or more). Slice sampling Neal (2003) was first adopted for nested sampling by Jasa & Xi-ang (2005) and popularized by PolyChord (Handley et al. 2015). Various slice sampling approaches were compared by Buchner (2022).

It is still unclear however how to choose the number of steps M . On the one hand, higher M induce a higher computational cost, which may be prohibitive. On the other hand, M must be chosen large enough so that the final point is sufficiently independent from the starting point (see also Salomone et al. 2018). If M is too small, the inference result and thus scientific conclusions may be wrong. It is thus essential to recognize such problematic nested sampling runs with diagnostics.

Diagnostics for nested sampling can be divided into two categories: visualisations, such as trace plots (Higson et al. 2019), and tests, which this paper focuses on. If the true answer is known, such as in analytic test distributions, the prior mass shrinkage can be tested directly (Buchner 2014), as well as the final evidence and posterior samples. Typically however the true answer is not known. Here, we can distinguish tests that are generic or specific to the likelihood-restricted prior sampling technique. For generic tests, consistency of Z across reruns (e.g. Feroz et al. 2013; Higson et al. 2019) is a basic check. However, consistency does not ensure a good run. Fowlie et al. (2020) recognized that a newly sampled live point should be inserted into to likelihood-ordered list of live points in a random place. The distribution of insertion orders should be uniform, which is checked with a K-S test. Buchner (2021) generalised this to the integer-based U-test, also applicable to dynamic nested sampling (Higson et al. 2017). For nested sampling based on rejection sampling, importance nested sampling has been proposed as an alternative estimator (Chopin & Robert 2010; Feroz et al.

* johannes.buchner.acad@gmx.com

2013). Disagreement between the importance nested sampling estimator and the classic nested sampling estimator is a useful indicator with the sampling (see e.g., Feroz et al. (2013); Nelson et al. (2020)). For step samplers, comparing the Z estimate when doubling M is a powerful diagnostic (Higson et al. 2017, 2019). A similar effect can be achieved by increasing the number of live points (Buchner 2023). Such reruns with substantially enlarged M or K incur a large computational cost. It would therefore be beneficial to diagnose an inference run by itself, rather than in comparison with other runs. Such a diagnostic is presented in this paper.

2. Method

2.1. Background

Generalising the idea of Fowlie et al. (2020), newly sampled points should be unremarkable in all their properties compared to the existing live points. Here, we consider the proximity to the existing live points, and focus in particular on the distance to the live point where the random walk was started. This is motivated by the common failure mode that a walk is not diffusing far away from the starting point.

In nested sampling, the starting point is a randomly chosen live point. Across iterations, therefore, multiple newly sampled points can originate from the same live point. If the walk is not going far, a clump of points near that live point appears. This is then apparent in the distribution posterior sample as graininess of the distribution. Such graininess has the fundamental property that the distance between properly sampled live points is different than the distance of the random walk. We use this to develop a test.

A performance indicator proposed for Random Walk Metropolis (RWM) is the expected square jump distance (ESJD) (Pasarica & Gelman 2010). It is defined as the mean square distance between one iteration and the next:

$$ESJD = E[JD^2] = E[\|\theta_{i+1} - \theta_i\|^2]$$

In particular, Pasarica & Gelman (2010) consider some univariate variable θ of interest, such as one model parameter. Then, the square jump distance is simply $(\theta_{i+1} - \theta_i)^2$. For a d -dimensional parameter position, the jump distance can be defined as the Euclidean distance. However, a local, decorrelated Mahalanobis distance may be more effective (see e.g. clustering and affine transformations in Higson et al. 2017). In this more general case, with a covariance matrix Σ , the jump distance (JD) is:

$$JD = \sqrt{(\theta_{i+1} - \theta_i)^T \Sigma^{-1} (\theta_{i+1} - \theta_i)}$$

To illustrate the behaviour of the ESJD, consider a RWM with a Gaussian proposal kernel. For a Gaussian proposal with a very small size, the ESJD is low. If the proposal kernel is too large, the Metropolis rule rejects most proposals and the chain remains stuck, again making the ESJD low. Based on this, Pasarica & Gelman (2010) optimize the kernel scale to maximize the ESJD. The ESJD is inversely related to the first-order auto-correlation of the random walk (Pasarica & Gelman 2010), which should be minimized for effective diffusion far away from the starting point.

In the context of nested sampling, Salomone et al. (2018) suggested optimizing the expected square jump distance (ESJD) with trial walks. Trials would need to be conducted at each nested sampling iteration, because the distribution is changing with each nested sampling iteration. Specifically, the prior volume becomes exponentially smaller.

2.2. Relative Jump Distance

Here, we develop a new diagnostic by relating the jump distance to the typical distance between live points. This is essential for nested sampling, because the sampled geometry, constrained by the evolving likelihood constraint, is changing in each iteration.

We define a reference distance to put the SJD in context. The reference distance should be a typical distance between live points. Following other works, for the numerical experiments in this paper, we work in a coordinate system defined in natural prior probability units (unit hyper-cube), and apply clustering and an affine whitening transformation that makes the live point sample covariance the unit diagonal matrix. This already provides a first normalisation of the jump distances. This is however insufficient, because the sample covariance is not equal to the covariance of the likelihood-restricted prior, and the likelihood-restricted prior may be more complex than an ellipsoidal distribution. To address the structure of the likelihood-restricted prior contour and its dimensionality-dependent edge behaviour, one can consider several choices, such as the typical nearest neighbor distance of the live points. However, complex likelihood-restricted prior geometries can make the nearest neighbor distance distribution multi-modal and therefore the mean and median nearest neighbour distance are unstable.

For a robust computation, we adopt as the reference distance the radius computed by the MLFriends algorithm (Buchner et al. 2014; Buchner 2016). This is found by splitting the live points into a training and a test sample, and identifying the nearest training point for each test point. The MLFriends radius r is then the maximum over all these nearest distances after B bootstrapping rounds. Here we adopt $B=30$. Appendix A presents Python code to compute r .

For the simplified mono-modal case of ellipsoidally distributed live points, Appendix A investigates the dependence of r on dimensionality and the number of live points, and finds a Mahalanobis distance of $r \approx 1$ in high dimensions. This is likely related to the ‘‘concentration of distances’’ effect (see e.g. Francois et al. 2007, for a review).

With the reference distance r in hand, we define the relative jump distance as:

$$RJD = JD/r \quad (1)$$

By definition of the bootstrapped r , multiple live points lie within the radius r . We therefore expect $RJD > 1$ for the majority of jumps, if the walk is effective.

2.3. Summary statistics

We observe the distribution of RJDs over the nested sampling run. To summarize the distribution, we track the fraction of jumps that exceed the reference distance ($f(RJD > 1)$) and the geometric mean RJD. As shown below, the RJD distribution is often log-normal. Problematic runs have a low-RJD tail. The geometric mean highlights such a tail better than an arithmetic mean or median, which would be dominated by the unproblematic large RJDs. The RJD can also be bi-modal. Consider for example a banana geometry in two dimensions. If there are enough live points, r describes the typical nearest neighbor distance, insensitive to the length of the banana. A good random walk traverses across the banana. A poor walk, with proposals only orthogonal to the banana, is stuck and only traverse approximately the width. The fraction of far jumps, $f(RJD > 1)$, diagnoses the ratio between good and poor proposals.

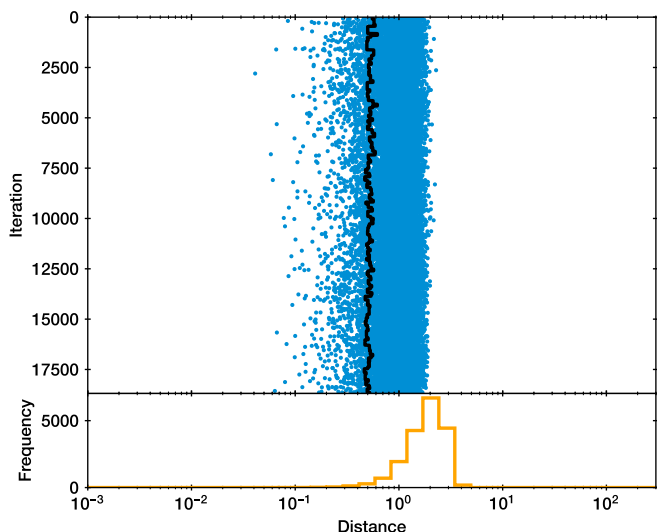


Fig. 1. Top panel: Jump Distance (blue) and reference Mahalanobis distance (black) at each nested sampling iteration for the nsteps=8 run. Most blue points are to the right of the black curve, i.e., $JD > r$. Bottom panel: The histogram of the ratio (relative jump distance, JD/r). The majority lies mostly above 1.

3. Results

We show the behaviour of our new diagnostic in several applications, which are specified by a d -dimensional prior probability distribution and a likelihood function. For each application, we run nested sampling with 400 live points until the dead points contain more than one per cent of the total estimated posterior weight. A sequence of runs is performed with d , $2 \times d$, $4 \times d$, $8 \times d$, etc. number of steps, where d is the number of model parameters. For simplicity and to clearly show the behaviour, we use a slice sampler that proposes along one randomly chosen parameter axis.

3.1. Gaussian

Integration of a Gaussian likelihood is a standard test problem: $L = \prod_{i=1}^d \text{Normal}(\mu_i, \sigma_i^2)$. The true marginal likelihood is $Z \approx 1$. We adopt standard uniform priors with $d=4$. The variation adopted here has different standard deviations for each parameter: $\sigma_i = 0.1 \times 10^{-(9 - \frac{\sqrt{d}}{2}) \times \frac{i-1}{d-1}}$. Thus, σ_i ranges from 10^{-9} to 10^{-1} . Additionally, the means are varied, avoiding a special place (such as the center) of the prior $\mu_i = \frac{1}{2} + \frac{1-5\sigma_i}{2} \times \sin \frac{i-1}{2d}$.

The jump distances of a nested sampling run is shown in Figure 1. The JD for each iteration are shown as blue dots and the reference distance r in black, both in whitened coordinates. r is close to 0.5 throughout. The bottom panel shows the RJD distribution. Figure 2 shows the RJD distribution for all nsteps runs. With 4 steps (blue histogram) the distribution is shifted to the left compared to the histograms with more steps. In all distributions, the majority have $RJD > 1$ (see figure legend), and the geometric mean RJD is also above 1. The inset in Fig. 2 presents the corresponding $\ln(Z)$ estimates from results from runs with different nsteps. These vary around the true value (0). Here both the $\ln(Z)$ calibration and the RJD distribution indicate acceptable runs.

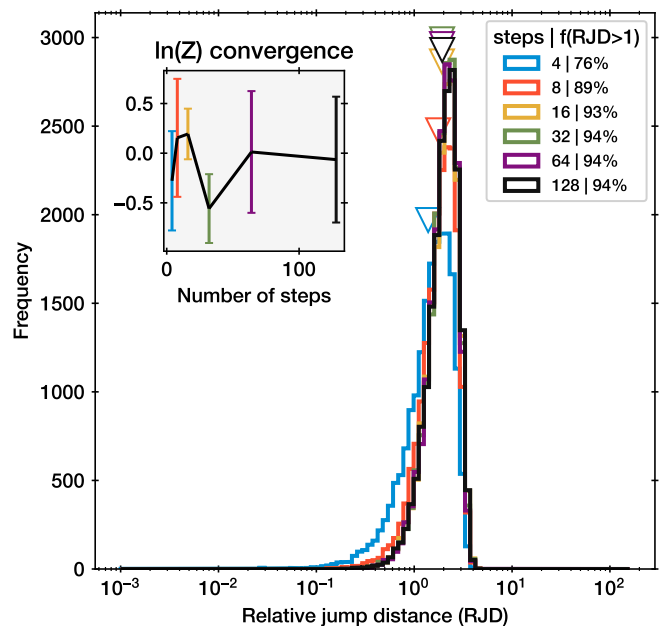


Fig. 2. Gaussian test likelihood run diagnostics. The inset shows evidence estimates (y-axis) for a sequence of nested sampling runs with different number of steps (x-axis). The RJD distribution for each is shown in the main panel. The distribution is bell-shaped in logarithmic units, but has a low-end tail, which is more pronounced when the number of steps is smallest (blue). The fraction of $RJD > 1$ is given in the legend with the number of steps. The geometric mean of RJDs for each run is shown near the respective histogram with the same color with downward-pointing triangles. Here, the means are all above 1 and the fractions above 50 per cent.

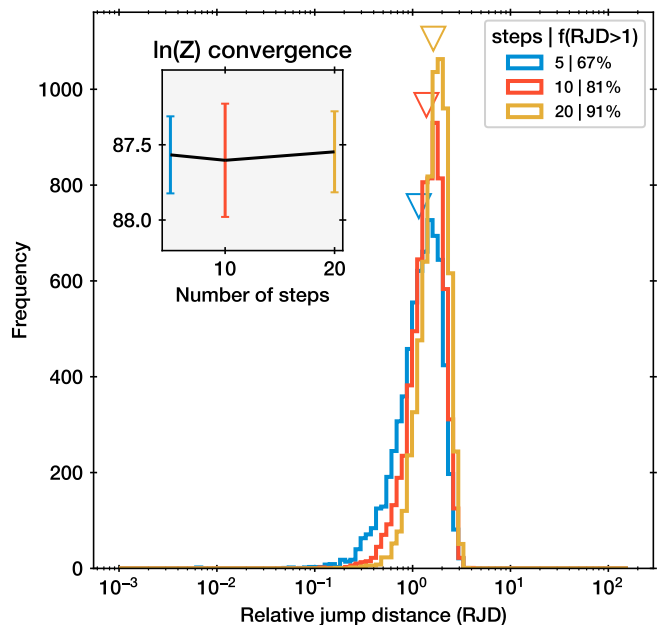


Fig. 3. Same as Fig. 2, but for a 5d box.

3.2. Box

We investigate a 5-dimensional non-ellipsoidal likelihood on a standard uniform prior. This is a sharply truncated Gaussian like-

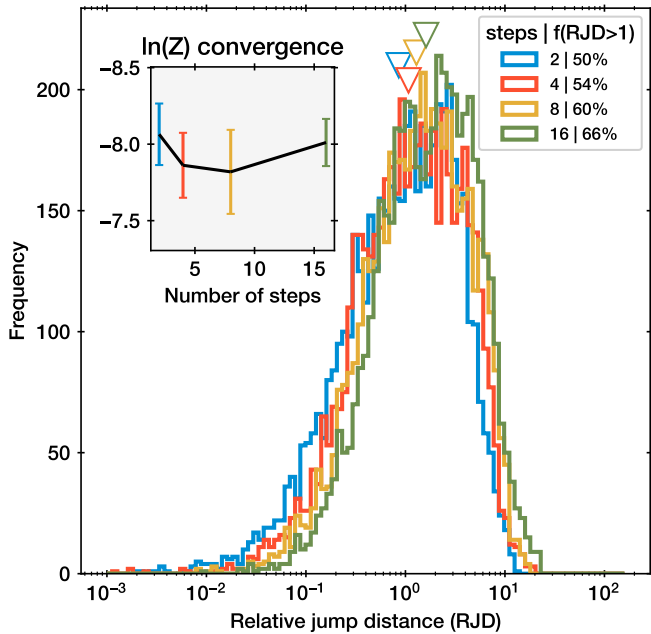


Fig. 4. Results from the banana-like Rosenbrock likelihood in 2d. Same as Fig. 2.

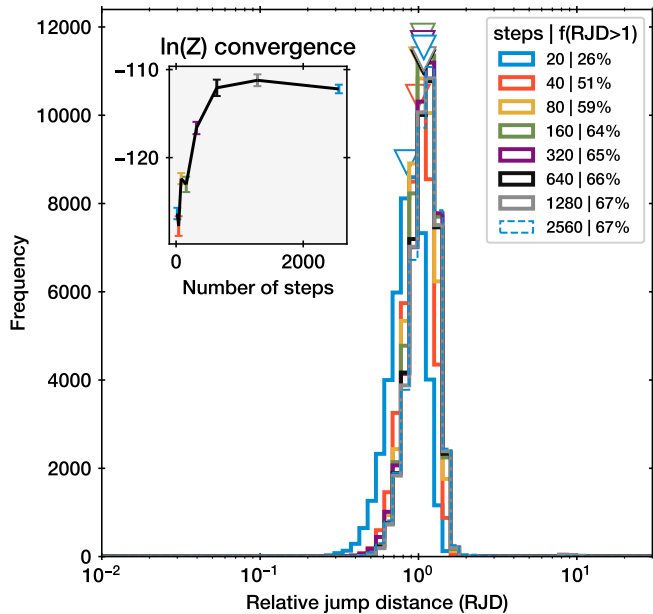


Fig. 5. Same as Fig. 4, but for the Rosenbrock likelihood in 20d. The RJD distribution (main panel) is bell-shaped in logarithmic units and shifts to the right with increased number of steps. The evidence estimate (inset) increases with the number steps until $nsteps=1024$.

likelihood: $\ln L = -\frac{1}{2} \times \left(\frac{\theta}{0.1}\right)^2 + 100 \times I[\delta < 0.1]$, where $\delta = \max_i |\theta_i|$ is the parameter with the largest deviation from zero.

The inset of Figure 3 shows no difference in evidence estimates with increasing number of steps. However, the histograms of RJD in Figure 3 inch further towards the right the more steps are used. With 20 steps, the vast majority of steps are at $RJD > 1$.

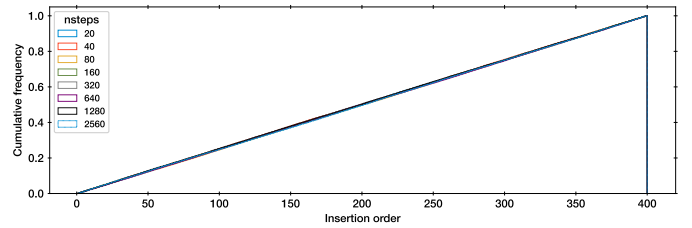


Fig. 6. Insertion order distribution for Rosenbrock runs in Fig. 5. In all cases, the deviation from a uniform distribution is insignificant ($p > 0.01$).

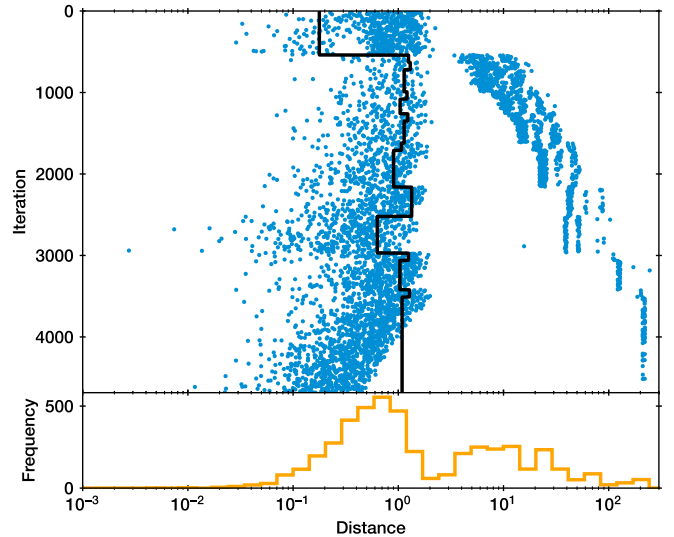


Fig. 7. Same as Fig. 1, but for the Eggbox likelihood analysed with $nsteps=8$. The reference distance (black curve) is low in the first 500 iterations, and most jump distances (blue dots) are larger. In the middle, the reference distance is near 1, and the jump distances are either near 1 or above 10. The bottom panel shows the resulting bi-modal RJD distribution.

3.3. Rosenbrock function

We next consider a higher-dimensional, and non-linearly degenerate likelihood. The Rosenbrock function is a standard test problem in optimization. It exhibits a banana-like degeneracy that can be difficult to navigate. We adopt the formulation $\log L = -2 \times \sum_{i=1}^{d-1} 100 \times (\theta_{i+1} - x_i^2)^2 + (1 - \theta_i)^2$ with uniform priors between -10 and +10 for each parameter.

For $d=2$, the main panel of Figure 4 shows no strong difference in evidence estimates, and the RJD histograms on the right are comparable. Most RJD are above 1. The $d=20$ case is more interesting. The inset of Figure 5 shows a strong change in evidence estimates as the number of steps is increased. Arguably, the result is not converged at fewer than 500 steps. The RJD histograms on the right also moves to the right with increasing number of steps, however, the effect is subtle from 40-180 steps. The mode of the RJD distribution is just above 1.

To complement these results, we also investigate the effectiveness of the insertion order statistic. Figure 6 presents a cumulative histogram of the insertion orders, which is indistinguishable from a uniform distribution. At all number of steps between the U test or KS test raise alarm about the results ($p > 0.01$).

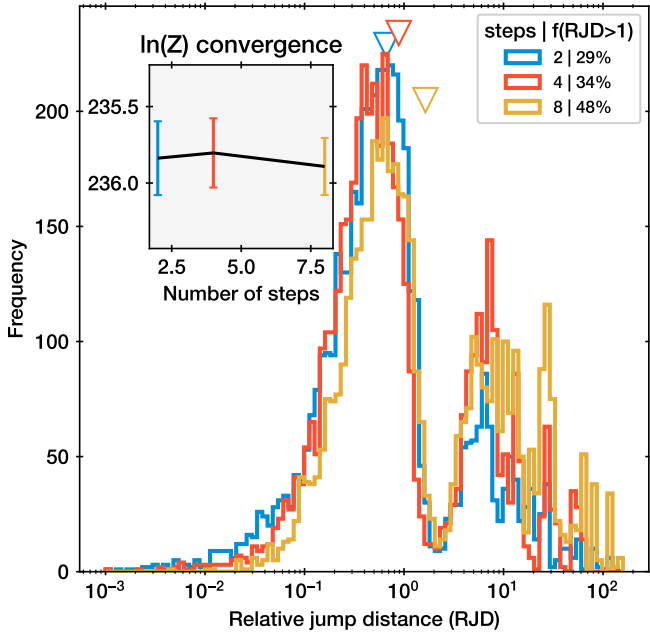


Fig. 8. The RJD distribution for the eggbox likelihood is bi-modal for all three runs (main panel). The evidence estimates in the inset are consistent within the error bars.

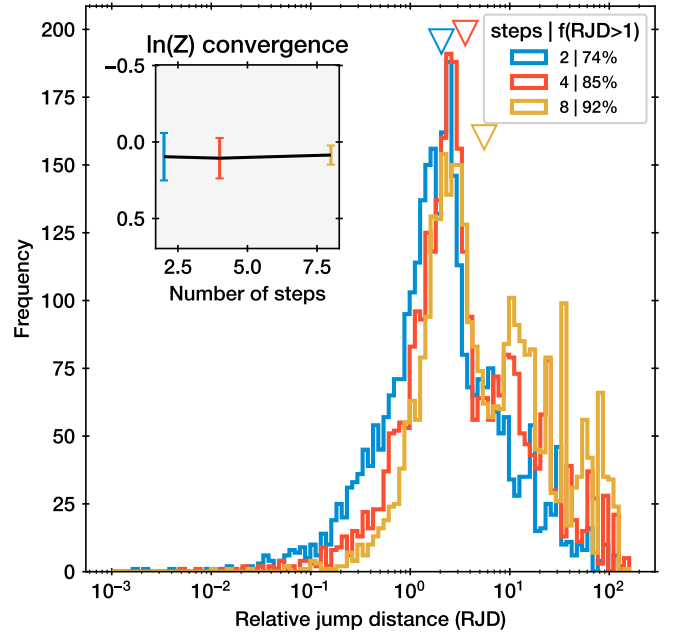


Fig. 9. LogGamma likelihood in 2d. The RJD distribution (main panel) is bi-modal at high number of steps. The tail at $\text{RJD} < 1$ is more pronounced at the lowest number of steps.

3.4. Eggbox

To investigate multi-modality, we adopt the two-dimensional Eggbox likelihood from [Feroz & Hobson \(2008\)](#). It is defined as: $\log L = (2 + \cos(5\pi \cdot \theta_1) \cdot \cos(5\pi \cdot \theta_2))^5$ with uniform priors for each parameter between 0 and 10π .

Here, the observed jump distances have a complex behaviour. Figure 7 shows the jump distances for a nested sampling run. Initially, the reference distance is indicating a typical neighbour distance of the uniformly distributed prior samples. After 500 iterations, the live points concentrate so that clusters can be identified, i.e., r indicates a typical distance within each cluster ($r \sim 1$). Some jumps are still possible across clusters ($\text{JD} \gg 1$), while most remain within ($\text{JD} \sim 1$). This leads to a bimodal distribution in RJD. The emerging RJD histograms on the bottom is then bimodal. Figure 8 compares the RJD histograms for runs with different number of steps. The evidence estimates in the inset of Fig. 8 show no significant variations.

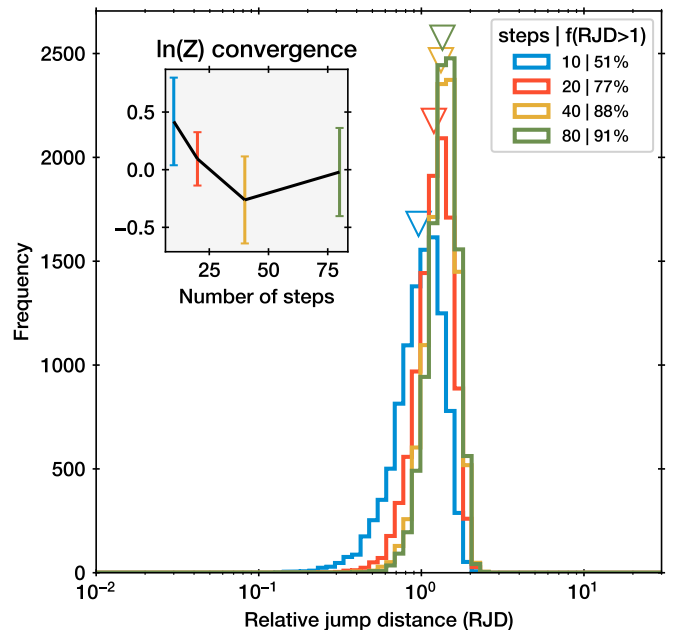


Fig. 10. The RJD distribution for the LogGamma likelihood in 10d is bell-shaped in logarithmic units and shifts to the right with increased number of steps. The results with 40 and 80 steps are very similar. The evidence estimates in the inset converge to the true value (0) at approximately 40 steps. At 20 steps or higher, the geometric mean indicated by the downward-pointing triangles lies above 1, and the fraction of RJD > 1 (listed in the legend) are above 75 per cent.

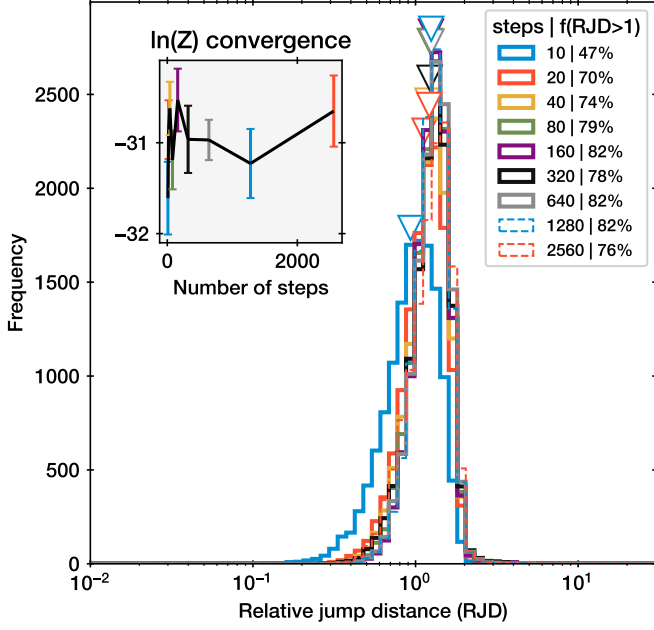


Fig. 11. Funnel likelihood in 10d. Same as Fig. 2.

3.5. LogGamma

A difficult multi-modal, non-ellipsoidal problem was introduced by [Beaujean & Caldwell \(2013\)](#), and is defined as:

$$g_a \sim \text{LogGamma}\left(1, \frac{1}{3}, \frac{1}{30}\right); n_c \sim \text{Normal}\left(\frac{1}{3}, \frac{1}{30}\right) \quad (2)$$

$$g_b \sim \text{LogGamma}\left(1, \frac{2}{3}, \frac{1}{30}\right); n_d \sim \text{Normal}\left(\frac{2}{3}, \frac{1}{30}\right) \quad (3)$$

$$L_1 = \frac{1}{2}(g_a(x_1) + g_b(x_1)); L_2 = \frac{1}{2}(n_c(x_2) + n_d(x_2)) \quad (4)$$

$$d_i \sim \text{LogGamma}\left(1, \frac{2}{3}, \frac{1}{30}\right) \text{ if } 3 \leq i \leq \frac{d+2}{2} \quad (5)$$

$$d_i \sim \text{Normal}\left(\frac{2}{3}, \frac{1}{30}\right) \text{ if } \frac{d+2}{2} < i \quad (6)$$

$$L = L_1 \times L_2 \times \prod_{i=3}^d d_i(x_i) \quad (7)$$

We test this problem in 2 and 10 dimensions, with parameters x_i assigned standard uniform priors. The true marginal likelihood is $Z=1$.

The RJD histograms in Fig. 9 is again complex, similar to the Eggbox. Going from the $nsteps=2$ (blue histogram) and the $nsteps=8$ case, a tail at low RJD disappears and a hump at $RJD \sim 10$ gains prominence. The latter is presumably related to jumps between modes. The evidence estimates are similar ($\ln(Z)=0.1$) and very close to the true value (0).

At higher dimensions, the evidence estimates are consistent with the true value (0) for runs with 20 steps or more (inset of Fig. 10). For 10 steps, the evidence is potentially over-estimated. The main panel of Fig. 9 shows that the histogram with 10 steps has the majority of RJD below 1, while at higher number of steps, the vast majority are above 1.

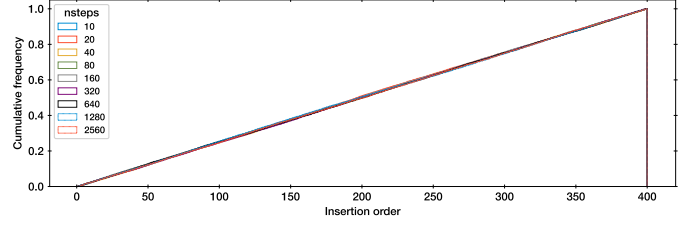


Fig. 12. Insertion order distribution for Funnel runs in Fig. 11. In all cases, the deviation from a uniform distribution is insignificant ($p>0.01$).

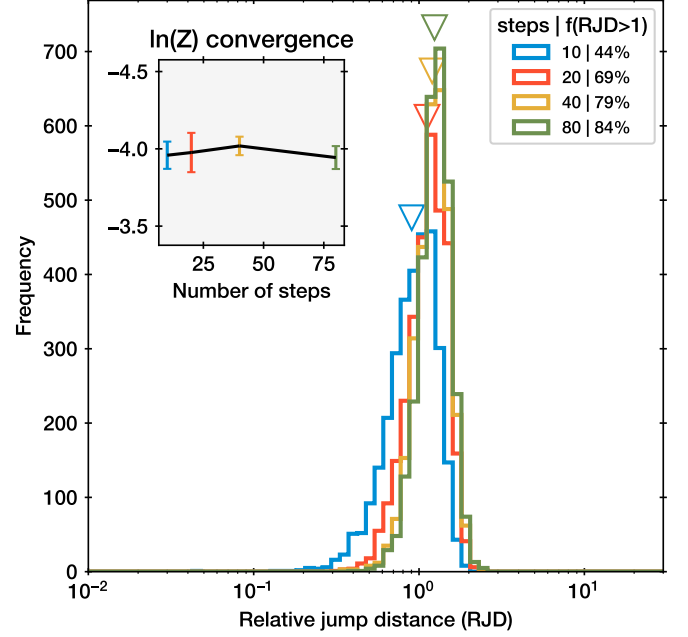


Fig. 13. The RJD distributions of the eight schools inference runs. These shift to the right with increasing number of steps. The evidence estimates shown in the inset overlap within the error bars.

3.6. Funnel

Neal's funnel is a standard test problem that represents features of hierarchical Bayesian models. Here we adapt the correlated version of [Karamanis & Beutler \(2020\)](#) with a covariance matrix M with diagonal elements $M_{ii} = \sigma$ and off-diagonals set to $M_{ij} = \gamma \times \sigma$ with $\gamma = 0.95$. Then the Gaussian likelihood is

$$\ln L = -\frac{1}{2} \left[(\mu M^{-1} \mu) / \sigma^2 \right] + d \ln(2\pi\sigma) + \ln \det(M)$$

with the standard deviation σ and locations μ_i being model parameters. We assign a standard normal prior to $\ln \sigma^2$ and uniform priors between -10 and 10 for each μ_i . This problem is tested in 10 dimensions (i.e., i from 1 to 9).

Figure 11 shows that the vast majority of RJD values lie above 1 if more than 10 steps are used. The evidence estimates in the inset are confined to a narrow range. Figure 12 shows a histogram of the insertion order distribution. These are indistinguishable from a uniform distribution for all cases. Of these three plots, the RJD distribution appears most sensitive to insufficient number of steps.

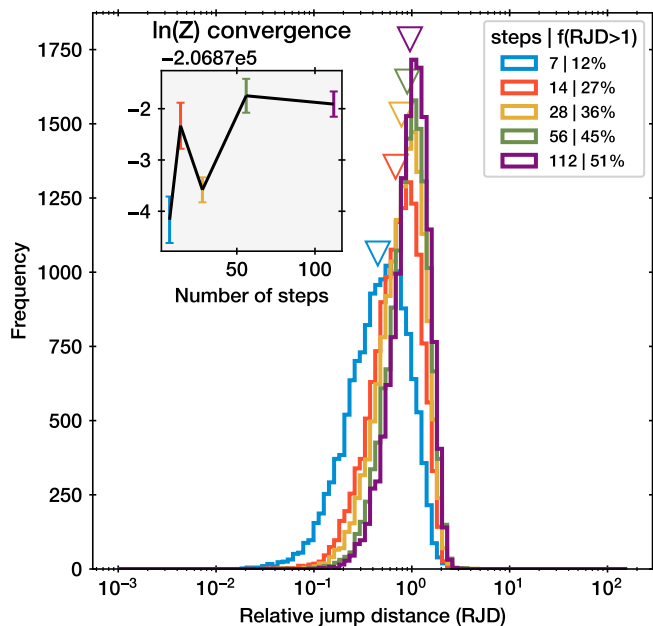


Fig. 14. The RJD distributions of GW170817 inference runs. These shift to the right with increasing number of steps. The evidence estimates are in the inset. They appear not converged at least with fewer than 56 steps.

3.7. Eight schools

We present a real-world inference problem from Rubin (1981), which obtained Gaussian measurements from eight schools of a treatment effect: $y \pm \sigma = 28 \pm 15, 8 \pm 10, -3 \pm 16, 7 \pm 11, -1 \pm 9, 1 \pm 11, 18 \pm 10, 12 \pm 18$. The mean treatment effect and the variance τ^2 over all schools is of interest. We therefore define a non-centered parameterization: $\ln L = \sum_i ((x_i \times \tau + \mu) - y_i)^2 / ((2\sigma_i^2))$ with the x 's assigned unit Gaussian priors. The hyper-parameters μ and τ are assigned a Gaussian and half-Cauchy distribution, respectively, with mean zero and scale 5. The results are presented in Fig. 13. They are very similar to the Gaussian and Box toy examples. There is no variation in $\ln(Z)$, but a noticeable change in RJD. The geometric mean RJD is 0.9 and 1.24 at the lowest and highest number of steps, respectively. The fraction $f(\text{JD} > r)$ rises from 44% to 84%.

3.8. Gravitational waves

The gravitational wave event GW170817 was observed by the LIGO Hanford, Livingston, and Virgo detectors, and inferred to be a binary neutron star inspiral (Abbott et al. 2017). We follow the PyCBC tutorial¹ and estimate the masses, inclination, distance, chirp time and position on the sky simultaneously with the marginalized phase Gaussian Noise likelihood (see Biwer et al. 2019) implemented in Nitz et al. (2024). For the sine of the inclination angle, a uniform prior is assumed. The prior for the position is uniform on the sphere. The prior on the distance is assumed to be uniform between 10 and 100 Mpc. The prior on the chirp mass and mass ratio q is assumed uniform between 1 and 2 solar masses. The prior on the time of coalescence is assumed uniform between 0.02 and 0.05s of the merger data set time stamp.

Figure 14 presents the RJD distribution of a sequence of runs. In the run with few steps (7; blue) the geometric mean lies

well below 1 and the $f(\text{RJD} > 1)$ is very low at 12%. Subsequent doubling of the number of steps increases the fraction up to 50%, with the geometric mean of RJD nearing 1. Runs with even more steps were not computed due to the computational cost.

The posterior distribution is presented in Fig. 15. The constraints are comparable to those published in Finstad et al. (2018), with minor differences likely arising due to the different, broader priors adopted here. With a low number of steps (7; blue), the distance posterior is much narrower than with the largest number of steps (112; red). This may be because the degeneracy between inclination, distance and time of coalescence could not be sufficiently explored. This demonstrates that the calibration of the number of steps can have consequences for the astrophysical interpretation of the event.

4. Discussion

We introduce a new, widely applicable diagnostic for nested sampling. It is easy to compute for low and high-dimensional inference tasks and does not require multiple nested sampling runs. The diagnostic is more sensitive than previously proposed tests.

We compared the RJD distribution, the insertion order U-test and $\ln(Z)$ convergence on several applications. The relative jump diagnostic is much more sensitive than the U-test. This is likely related to using more information, namely d -dimensional spatial coordinates rather than likelihood quantiles. The relative jump diagnostic appears to be at least as sensitive as observing $\ln(Z)$. An important difference is that, rather than requiring a sequence of runs, the fraction of $\text{RJD} > 1$ provides a sensitive test of a performed or on-going run in isolation.

The toy problems suggest that in mono-modal posteriors the nested sampling run can be considered trustworthy when $f(\text{JD} > r)$ is above 50 per cent, and the geometric mean of RJD is above 1. Intuitively, the former criterion says that the median jump distance exceeds the typical distance between live points.

The expected relative jump distance can be over-estimated. If the number of live points is low and/or the dimensionality high, clusters and local structures may be unrecognizable when computing the typical neighbour distance. Similarly, if the reference distance is only computed every n th iteration, then the moment when a likelihood-restricted prior becomes multi-modal and the modes cannot be traversed any longer by jumps may be missed. Then the jump distance may be surprisingly low, although the walk has diffused well. We observe such behaviour with the multi-modal Eggbox and Loggamma toy problems.

Our recommendation to practitioners therefore is: (1) If $\text{RJD} > 1$ for the majority of samples, then the nested sampling result can be trusted. (2) Otherwise rerun with twice as many steps. If either the RJD distribution changed, or the Z estimate changed significantly, go to (1). Otherwise, the result may be acceptable. The cautious practitioner should double the number of steps once more than seems necessary.

The RJD diagnostic compares the new-born live point to the starting point of its random walk. This makes it specific to step sampling-based nested samplers. A generalization would be to consider the distance of the new-born point to its nearest existing live point, rather than the starting point. Such a generalization could be implemented without modification to existing nested samplers. Our diagnostic is a stronger form, because it uses the most correlated point. Implementation in existing nested sampling packages is easy and demands little additional resources, since only the distance between starting and final point needs

¹ Tutorial 0 from <https://github.com/gwastro/PyCBC-Tutorials/>

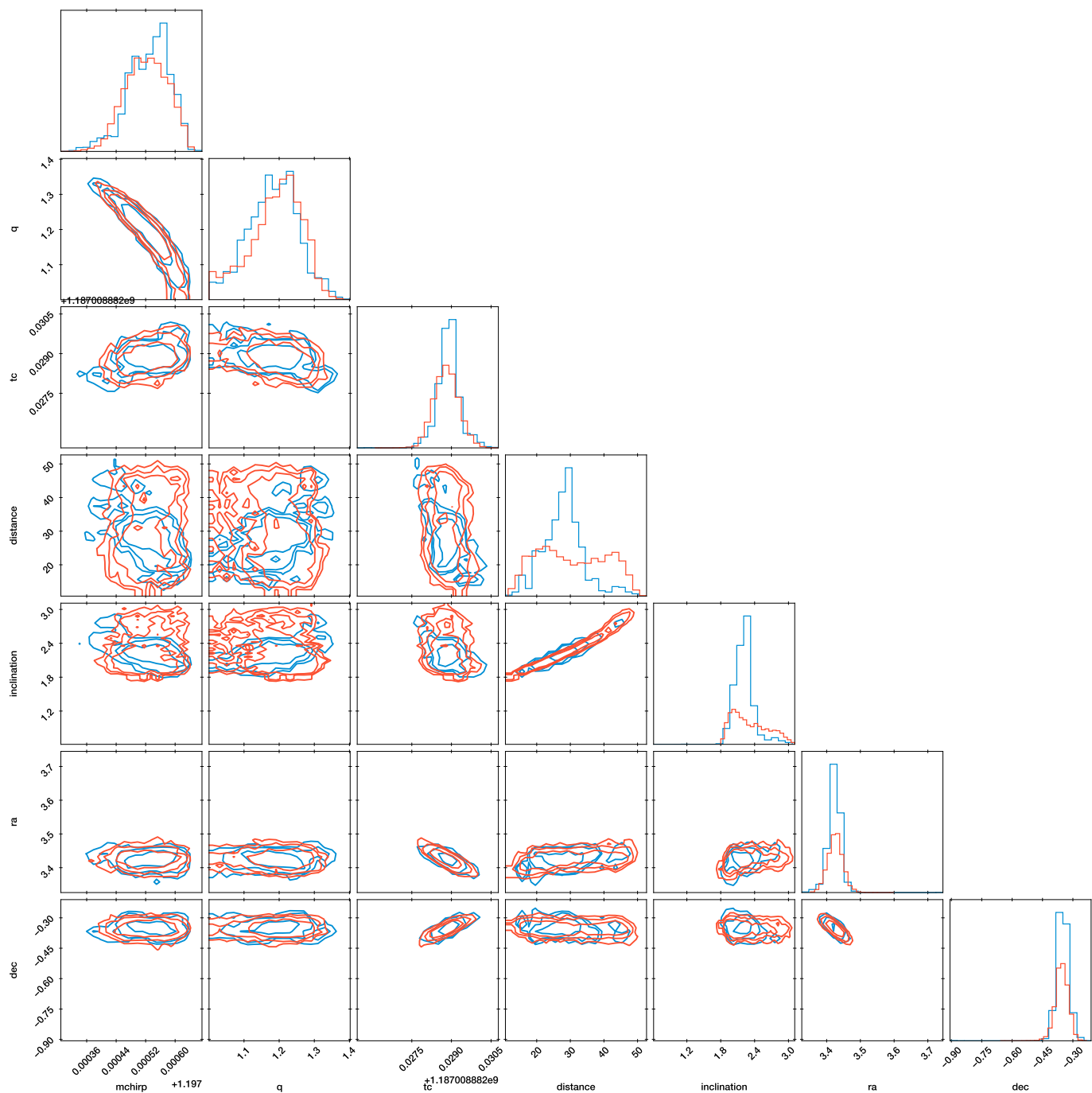


Fig. 15. Corner plot for GW170817. Red posteriors are from a run with 112 steps, while blue posteriors are from a run with 7 steps. The contours include 39.3%, 86.4% and 95% of the posterior probability distribution. Inclination, RA and Dec are given in units of π .

to be stored. The RJD diagnostic is implemented in *UltraNest*² from version 4.1.

Future work will explore ways to adapt the number of steps during a nested sampling run. Preliminary implementations in *UltraNest* are available which increase the number of steps after each iteration where $RJD < 1$, and decrease it after each iteration where $RJD > 1$. An alternative approach would be to use Snowballing nested sampling (Buchner 2023), i.e., choose a fixed number of steps and bulk up the number of live points in likelihood ranges where $f(JD > r)$ was low. As the density of live points

increases, the typical neighbour distance r decreases, which increases RJD without the need to discard existing chains.

Acknowledgments

I thank Will Handley for insightful conversations, which were hosted by the Kavli Institute for Cosmology in Cambridge, UK.

References

- Abbott, B. P., Abbott, R., Abbott, T. D., et al. 2017, *Phys. Rev. Lett.*, 119, 161101
 Ashton, G., Bernstein, N., Buchner, J., et al. 2022, arXiv e-prints, arXiv:2205.15570

² <https://johannesbuchner.github.io/UltraNest/>

- Beaujean, F. & Caldwell, A. 2013, ArXiv e-prints [arXiv:1304.7808]
- Biwer, C. M., Capano, C. D., De, S., et al. 2019, *PASP*, 131, 024503
- Buchner, J. 2014, *Statistics and Computing*, 1
- Buchner, J. 2016, *Statistics and Computing*, 26, 383
- Buchner, J. 2020, UltraNest v2.2.1, <https://johannesbuchner.github.io/UltraNest/>
- Buchner, J. 2021, arXiv e-prints, arXiv:2101.09675
- Buchner, J. 2022, *Physical Sciences Forum*, 5
- Buchner, J. 2023, *Physical Sciences Forum*, 9
- Buchner, J., Georgakakis, A., Nandra, K., et al. 2014, *A&A*, 564, A125
- Chopin, N. & Robert, C. P. 2010, *Biometrika*
- Feroz, F. & Hobson, M. P. 2008, *MNRAS*, 384, 449
- Feroz, F., Hobson, M. P., & Bridges, M. 2009, *MNRAS*, 398, 1601
- Feroz, F., Hobson, M. P., Cameron, E., & Pettitt, A. N. 2013, ArXiv e-prints [arXiv:1306.2144]
- Finstad, D., De, S., Brown, D. A., Berger, E., & Biwer, C. M. 2018, *ApJ*, 860, L2
- Fowlie, A., Handley, W., & Su, L. 2020, arXiv e-prints, arXiv:2006.03371
- Francois, D., Wertz, V., & Verleysen, M. 2007, *IEEE Transactions on Knowledge and Data Engineering*, 19, 873
- Handley, W. J., Hobson, M. P., & Lasenby, A. N. 2015, *MNRAS*, 453, 4384
- Higson, E., Handley, W., Hobson, M., & Lasenby, A. 2017, ArXiv e-prints [arXiv:1704.03459]
- Higson, E., Handley, W., Hobson, M., & Lasenby, A. 2019, *MNRAS*, 483, 2044
- Jasa, T. & Xiang, N. 2005, in *American Institute of Physics Conference Series*, Vol. 803, *Bayesian Inference and Maximum Entropy Methods in Science and Engineering*, ed. K. H. Knuth, A. E. Abbas, R. D. Morris, & J. P. Castle, 189–196
- Karamanis, M. & Beutler, F. 2020, arXiv e-prints, arXiv:2002.06212
- Neal, R. M. 2003, *Ann. Statist.*, 31, 705
- Nelson, B. E., Ford, E. B., Buchner, J., et al. 2020, *AJ*, 159, 73
- Nitz, A., Harry, I., Brown, D., et al. 2024, gwastro/pycbc: v2.3.3 release of Py-CBC
- Pasarica, C. & Gelman, A. 2010, *Statistica Sinica*, 343
- Rubin, D. B. 1981, *Journal of Educational Statistics*, 6, 377
- Salomone, R., South, L. F., Drovandi, C. C., & Kroese, D. P. 2018, arXiv e-prints, arXiv:1805.03924
- Skilling, J. 2004, *AIP Conference Proceedings*, 735, 395
- Speagle, J. S. 2020, *MNRAS*, 493, 3132

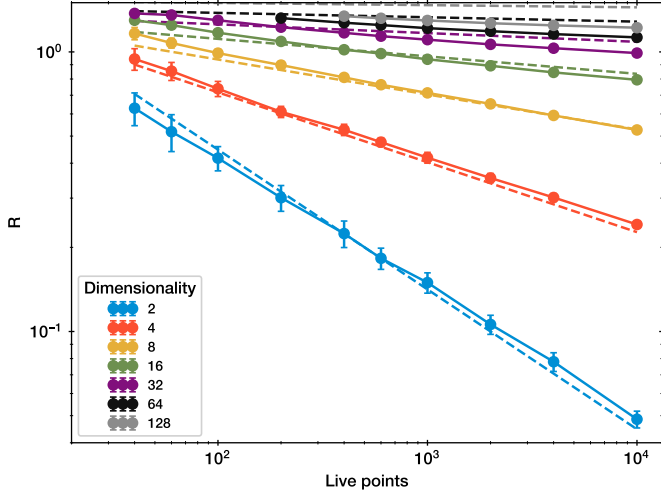


Fig. A.1. Scaling of reference radius with number of live points and dimensionality. Each error bar summarizes the mean and standard deviation from 40 simulations. The dashed curves is Eq. (A.1). This approximates most data points, but there are deviations in high dimensions and low number of live points.

Fig. A.2. Python code to compute MLFriends radius. Function `compute_radius` is called with an array of live points.

```

from ultranest.mlfriends import MLFriends,
AffineLayer
def compute_radius(live_points):
    # start with a Euclidean distance
    layer = AffineLayer()
    # run MLFriends, find radius
    region = MLFriends(live_points, layer)
    r, _ = region.compute_enlargement()
    # Create Mahalanobis distance, considering
    clusters within distance r
    layer2 = layer.create_new(live_points, r)
    # run MLFriends and return radius
    region2 = MLFriends(live_points, layer2)
    r2, _ = region2.compute_enlargement()
    return r2**0.5

```

Appendix A: Reference distance for ellipsoids

To illustrate the behaviour of the defined reference distance, we can consider ellipsoidal contours. If we consider that an ellipsoid volume V that is segmented into K equal sub-volumes with a volume proportional to r^d , then $V \propto K \times r^d$. For fixed V , we find the scale between neighbours r scales as $r \propto K^{-\frac{1}{d}}$.

We perform numerical experimentation sampling K points from an ellipsoid in up to 128 dimensions. We compute r with the code listed in Fig. A.2. The found r values are presented in Fig. A.1. We also plot the relation:

$$r = (20/K)^{\frac{1}{d}} \times (d/2)^{0.1} \quad (\text{A.1})$$

As discussed above, the first term is the volumetric distribution by the K live point in a d -dimensional hyper-sphere. The weak second term is likely related to the empirical whitening transformation failing to accurately identify the true whitening transform in high dimensions.

In high dimensions we find that r lies between 1.2 and 1.3, independent of the number of live points. Likely this is related to the number of bootstrapping rounds. $r = 1$ intuitively corresponds to the Mahalanobis distance of any ellipsoid axis. If we were to adopt $r = 1$, the RJD criterion would become more optimistic about the achieved jump length. In more realistic settings than the ellipsoidal contours considered here, r may be substantially different.